THE ASTROPHYSICAL JOURNAL, 494:202–210, 1998 February 10

SPECTROSCOPY OF THE NUCLEAR EMISSION-LINE REGIONS OF THE TWO NEWLY DETECTED SEYFERT 1 GALAXIES F10.01 AND A08.12

ALBERTO RODRÍGUEZ-ARDILA,[1,2] AND MIRIANI G. PASTORIZA
Departamento de Astronomia, IF-UFRGS, CP 15051, CEP 91501-970, Porto Alegre, RS, Brazil; alberto@if1.if.ufrgs.br
AND
J. MAZA[3]
Departamento de Astronomía, Universidad de Chile, Casilla 36-D, Santiago, Chile
Received 1996 November 11; accepted 1997 September 19

ABSTRACT

Long-slit medium-resolution spectra are used to study the continuum and ionization properties of the gas in the Seyfert 1 galaxies F10.01 and A08.12. We find that the nuclear underlying continuum can be described by a power law. In addition to this component, Balmer continuum (Bac) and high-order Balmer lines can fit the apparent excess of emission extending from 3900 Å to the blue end of the spectra. The observed Bac flux in A08.12 is about 9 times as strong as Hβ, stronger than that predicted by most photoionization models. From the analysis of the Fe II emission, we found Fe II λ4570/H$\beta \sim 1$ in F10.01, leading us to consider this object as a strong Fe II emitter. Broad and symmetrical Balmer lines are observed in A08.12, while strongly asymmetrical ones are observed in F10.01, with the full width at zero intensity (FWZI) around 15,000 km s^{-1}.

We interpret the above results as evidence for broad-line region (BLR) gas exposed to the anisotropic UV radiation emitted by a thin disk combined with an isotropic X-ray source. Such a model could explain observational differences like strong Fe II and weak Bac and He I λ5875 emission in F10.01, and strong Bac and He I λ5875 and weak Fe II in A08.12, as due to an angular dependence of emission-line intensities.

The narrow-line region (NLR) of both objects shows strong high-ionization lines and $T_{[\mathrm{O\,III}]}$ temperatures that cannot be reproduced simultaneously using single-component ionization-bounded photoionization models. We explore here the possibility of a NLR composed of a combination of matter-bounded (MB) and ionization-bounded (IB) clouds. In this scheme, the MB component is responsible for most of the high-excitation lines, including the [O III] emission, while the IB clouds, photoionized by the radiation leaking the MB component, are located 140 times more distant from the central source than the MB clouds and show a much lower excitation. Using this scheme, we can successfully solve the "temperature problem" and obtain much stronger excitation lines, in accordance with our observations.

Subject headings: galaxies: individual (F10.01, A08.12) — galaxies: nuclei — galaxies: Seyfert

1. INTRODUCTION

Seyfert 1 galaxy spectra are characterized by the breadth of their continuum radiation, which is bright across up to 10 decades in frequency, from the X-rays to the radio domain. Superposed on this continuum, there are broad permitted emission lines with widths typically ranging between 5000 and 10,000 km s^{-1}, and narrow permitted and forbidden lines that are almost always narrower than 1000 km s^{-1}. In addition, broad bumps of emission at both sides of Hβ, produced by the merging of several Fe II multiplets and a broad emission feature in the near-UV (the so-called small blue bump) are also usually found in these objects. During the course of the Calán-Tololo Survey (Maza et al. 1989, 1992, 1994), several galaxies with the above features were identified and therefore classified as Seyfert 1 galaxies, most of them previously unknown.

In this paper we study F10.01 and A08.12, two of these newly discovered Seyfert 1 galaxies that display apparently different spectroscopic properties related to the presence of Fe II emission lines and Balmer continuum. We show that these differences can be explained as due to intrinsic changes resulting from the variation in the illumination angle of the BLR clouds. Measurement of the narrow-line spectrum allows several important and unique investigations regarding the physical conditions of the emission-line gas. In particular, the temperature ($T_{[\mathrm{O\,III}]}$) of both galaxies, inferred from the line ratio $R_{[\mathrm{O\,III}]}$ (=[O III] λ4363/[O III] λ5007), exceeds the equilibrium temperature predicted by photoionization models calculated with densities $n < 10^4$ cm^{-3} and solar abundance. Here we show that the inclusion of matter-bounded clouds with densities $n \gtrsim 10^6$ cm^{-3} can reproduce the observed values of $R_{[\mathrm{O\,III}]}$ and give a better match to the observed narrow-line region (NLR) spectra.

F10.01 is a luminous galaxy ($M_B = -22$) with elliptical-like morphology on the ESO-SERC J plates. Its apparent major diameter, as measured from the plate, is 27″, corresponding to a projected diameter of 40 kpc at the galaxy distance of 313 Mpc. A08.12, located at a distance of 119 Mpc, has a moderate luminosity ($M_B = -20$) and a major projected diameter of 17 kpc. It looks like an early-type

[1] CNPq Fellow.
[2] Visiting Astronomer at Complejo Astronómico El Leoncito (CASLEO) Observatory, which is operated under agreement between the Consejo Nacional de Investigaciones Científicas y Técnicas de la República Argentina and the National Universities of La Plata, Córdoba, and San Juán.
[3] Visiting Astronomer at the Cerro Tololo Inter-American Observatory, operated by Associated Universities for Research in Astronomy, Inc., under contract to the National Science Foundation.

spiral in the *B* ESO plates. A search in the *IUE* and *EXOSAT* database shows that they have not been observed in the UV and X-ray spectral regions. Also, there is no available information about them in the radio domain.

In § 2 we describe the observations. The continuum decomposition applied to the galaxies is described in § 3. In § 4 we study the emission-line profiles and the physical properties of the line-emitting regions. Conclusions are presented in § 5. A value of the Hubble constant of $H_0 = 75$ km s^{-1} Mpc^{-1} has been assumed throughout this paper.

2. OBSERVATIONS AND DATA REDUCTION

Long-slit spectra of F10.01 and A08.12 were obtained in 1992 October with the 4 m telescope at the Cerro Tololo Inter-American Observatory (CTIO), equipped with a Ritchey-Chrétien spectrograph and a CCD detector. They cover the rest-wavelength range 3200–6850 Å and have a resolution of ~8 Å. The observations were taken using a slit width of 2″ oriented in the east-west direction and an exposure time of 600 s. For flux calibration, spectrophotometric standards of Stone & Baldwin (1983) were observed. Data reduction was carried out at the CTIO La Serena Computing Center using the IRAF software. Sky subtraction was performed by taking parts of the sky where no flux from the objects themselves was observed. Extractions were made by summing up the observed signal along the central 12 pixels on the two-dimensional frames. The data of Burstein & Heiles (1984) suggest that reddening due to the Galaxy should be small in the direction of both objects, so they were not corrected for Galactic extinction. From the position of the most intense emission lines, we have obtained a radial velocities of 23,500 ± 100 km s^{-1} and 8900 ± 40 km s^{-1} for F10.01 and A08.12, respectively. Heliovelocity corrections were not applied to the above values, since they are within the error bars. Figure 1 shows the reduced spectra already corrected for redshift.

In addition to the above spectra, a high signal-to-noise ratio (S/N) spectrum of the Fe II emitter Seyfert 1 galaxy I Zw 1 (PG 0050+124) was obtained with the CASLEO 2.15 m telescope on 1996 August 12 using a TEK 1024 × 512 CCD detector and a REOSC spectrograph. The spectrum covers the rest-wavelength range 3500–6800 Å and was taken using a 2″.5 wide long-slit oriented in the east-west direction with an integration time of 600 s. The two-dimensional frame was bias subtracted, divided by flat field, sky subtracted, wavelength calibrated, and then transformed in energy flux units using the IRAF software. Standard stars LTT 7987 and LTT 1020 from Stone & Baldwin (1983) were observed in order to derive the flux calibration. A one-dimensional spectrum was extracted by binning together 10 pixels from the nuclear and adjacent regions and was then corrected for redshift and $E(B-V)$ using the values reported by Marziani et al. (1996). The aim of this observation is described in § 3.2

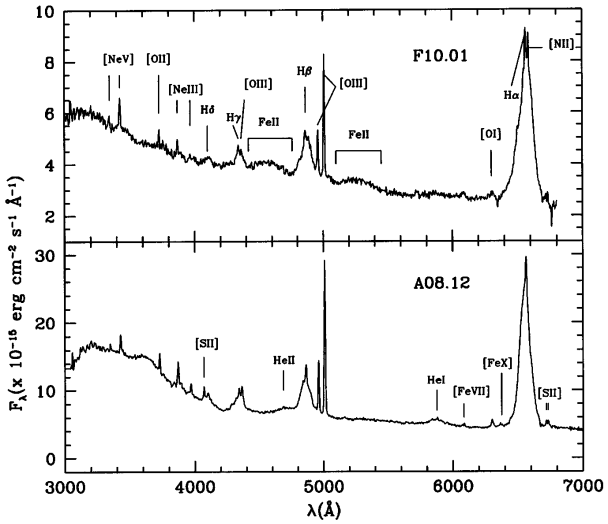

FIG. 1.—Observed spectra of the F10.01 (*upper panel*) and A08.12 (*lower panel*) Seyfert 1 galaxies in the rest system of the objects. Note the large widths of the permitted lines, the strong Fe II emission in F10.01, and the remarkable near-UV excess emisson in A08.12.

3. CONTINUUM ANALYSIS

It is widely known that the optical emission spectrum of a Seyfert 1 galaxy is composed of a combination of (1) an underlying stellar contribution from the host galaxy and (2) a nonstellar continuum, associated with the central engine. Additional features, such as the Balmer continuum emission and the pseudocontinuum produced by the merger of numerous Fe II multiplets are usually present. In F10.01 and A08.12 the contribution of the stellar population to the total continuum cannot be reliably determined, since absorption features like Ca II K λ3933, CN G λ4301, and Mg + Mg H λ5175 are rather small, almost reduced to noise level. This makes the identification of the correct template for the host galaxy a very uncertain procedure. Therefore, no effort was made to subtract this contribution from these objects.

3.1. *Power-Law Component*

A nonstellar continuum, well described by a power law (PL) $F_\lambda = k\lambda^\alpha$, is present in both spectra and is the dominant component of the continuum emission. Estimating the slope of the PL demands choosing points in the continuum free of emission lines or other sources of emission. However, the presence of many broad lines, the wings of which often overlap and blend, makes the determination of the true continuum an arduous task. Usually the regions around 4600, 5400, and 5900 Å and redward of Hα are free of emission lines, so they are useful to determine the true level of the continuum. In the upper panels of Figures 2 and 3 we show the underlying power-law fit applied to F10.01 and A08.12, respectively, using the *nfit1d* task of the STSDAS package of IRAF. The spectral index α of the PL and the integrated optical flux in the range 3200–7000 Å carried out by this component are listed in Table 1. The errors associated with the fit were directly estimated from the *nfit1d* task

TABLE 1

CONTINUUM DECOMPOSITION AND FLUXES[a]

Feature	F10.01	A08.12
Power law	13.0 ± 0.3	24.5 ± 0.6
Fe II λ4570	0.14 ± 0.01	...
Fe II (optical)	0.55 ± 0.05	...
Bac (3200–3646) + $\sum F_{\mathrm{H15}-n_{\mathrm{lim}}}$	0.25 ± 0.09	5.7 ± 0.3
Bac (total)	0.39 ± 0.11	9.6 ± 0.5
Bac model parameters: τ, T_4 (K)	1.0, 1.0	0.0, 1.2
Power-law index	−1.10 ± 0.05	−1.20 ± 0.06

[a] Fluxes in units of 10^{-12} ergs s^{-1} cm^{-2}.

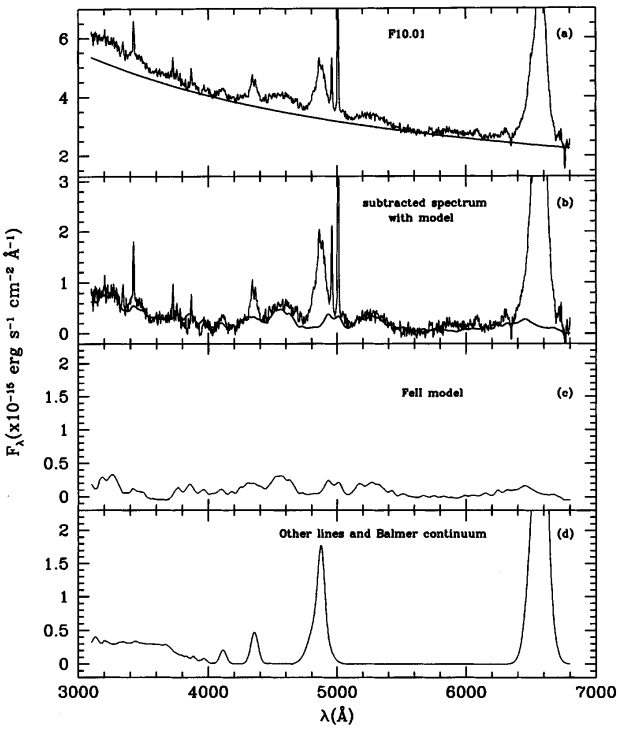

FIG. 2.—Continuum decomposition applied to F10.01. (*a*) Observed spectrum along with the power-law fit to the underlying continuum. (*b*) The same spectrum with the power law subtracted and superposed, the synthetic continuum spectrum, composed of the Fe II plus the Bac templates. The Fe II spectrum and the Balmer continuum combined with other broad lines are shown in (*c*) and (*d*), respectively.

itself, which makes use of the downhill simplex minimization method ("amoeba") to minimize the χ^2. After subtracting the power-law spectrum, we were confronted with two problems of different nature: the pseudocontinuum created by the blending of several Fe II multiplets and the Balmer continuum emission.

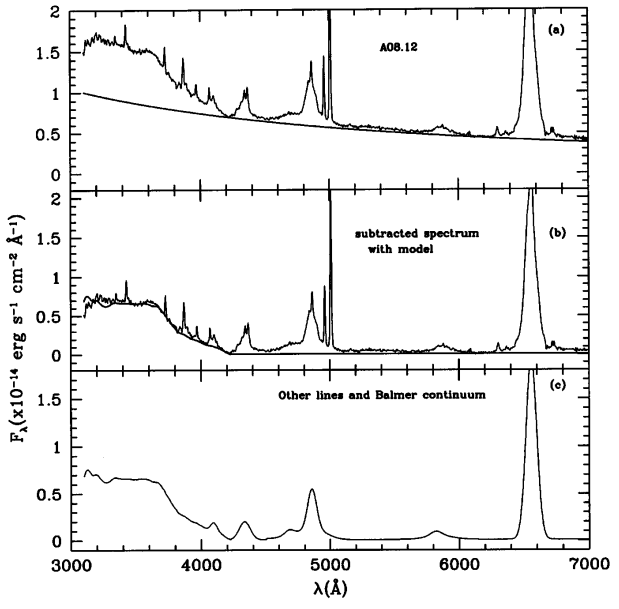

FIG. 3.—Continuum decomposition applied to A08.12. (*a*) Observed spectrum along with the power-law fit to the underlying continuum. (*b*) The same spectrum with the power law subtracted and with the synthetic Balmer continuum model superposed. (*c*) Balmer continuum combined with other broad lines.

3.2. Fe II *Emission*

In a close inspection of the F10.01 spectrum in Figure 1, one can easily see two conspicuous features in the form of broad bumps at the intervals $\lambda\lambda$4450–4750 and $\lambda\lambda$5150–5400, denoting the presence of a very rich Fe II spectrum. These bumps result from the merging of several Fe II emission multiplets (Wills, Netzer, & Wills 1985, hereafter WNW). In addition, there is a strong Fe II multiplet (42), consisting of three lines at $\lambda\lambda$4924, 5018, 5169, and many other multiplets located in the blue region. The origin of this emission constitutes one of the puzzles in understanding the spectra of active galactic nuclei (AGNs). It is known that these lines arise from the six odd-parity terms that lie between 4.76 and 5.91 eV above the ground state (Kwan et al. 1995). Collisional excitation of these six terms, followed by permitted radiative decays to metastable even-parity terms, is the major source of Fe II emission.

Determining the strength of the Fe II emission lines is not an easy task. These lines are usually heavily blended, complicating a good determination of the continuum level. There is also the possibility of contamination by the strong wings of the Balmer lines, specially those of Hβ, so care must be taken in the deblending process.

In order to determine and measure the Fe II blends in the wavelength interval 3600–6800 Å, we followed the empirical method developed by Boroson & Green (1992). It consists of constructing a Fe II template spectrum by removing the lines which are not of Fe II from the spectrum of I Zw 1, a Seyfert 1 galaxy widely known for the strength of the Fe II emission and the narrowness of its "broad lines." For this purpose, a high S/N spectrum of I Zw 1 covering the spectral range 3500–6800 Å was taken (see § 2). A synthetic Fe II spectrum from the grid of WNW was employed to measure the strength of the Fe II lines located in the interval 3200–3600 Å. A good agreement between this synthetic spectrum and the I Zw 1 template in the spectral range 3600–6800 Å is observed. Nonetheless, we prefer the I Zw 1 template for this zone because it includes some optical lines not present in the WNW spectrum. The line profiles of both Fe II templates were broadened separately by convolving them with a Gaussian profile having a FWHM equal to that of the Hβ line in F10.01 and scaled to match the observed Fe II emission of that galaxy. Since there is no significant Fe II emission around 3670 Å, this region was used to merge the two Fe II spectra. Figure 2*b* shows the resulting Fe II template superposed on the observed Fe II emission in F10.01.

We did not find concrete evidence for the presence of Fe II emission either in the optical region or in the 3000–3600 Å interval in the A08.12 galaxy. One may be tempted to treat the weak feature in excess of the PL, located redward of [O III] λ5007 (see Fig. 3*b*), as due to Fe II but it extends too much toward the red ($\sim$5600 Å) to be attributable to this ion. Also, there is no observable Fe II emission of comparable strength at the blue side of Hβ. One might argue that such an emission is hindered by the strong He II λ4686 line but the peak of the Fe II λ4570 feature would lie precisely in the far red wing of the He II profile, so if Fe II were present, it could not have been overlooked. The absence of Fe II in the optical does not imply weak Fe II emission in the UV (WNW). However, no evidence of significant Fe II lines in the interval 3000–3600 Å was observed in A08.12, leading

us to conclude that A08.12 shows no Fe II within the error uncertainties of our measurements.

From the final Fe II template we have estimated Fe II $\lambda 4570/\mathrm{H}\beta = 0.9 \pm 0.1$ and Fe II opt/H$\beta = 3.6 \pm 0.4$ in the F10.01 galaxy. By Fe II $\lambda 4570$ we mean the integrated flux of the Fe II complex $\lambda\lambda 4430$–4750. It is considered the most important and reliable blend to measure, since it not only scales with the total strength of the optical Fe II emission but also accounts for about 25% of the total optical Fe II emission (Collin-Souffrin et al. 1986). Fe II opt, on the other hand, indicates the integrated flux of the optical Fe II lines located in the interval 3500–6800 Å.

According to the value found for the Fe II $\lambda 4570/\mathrm{H}\beta$ ratio in F10.01, this galaxy can be considered as a strong Fe II emitter (Fe II $\lambda 4570/\mathrm{H}\beta \geq 1$, following Lípari, Terlevich, & Macchetto 1993). This result gains additional importance when we look at the FWHM of the broad Balmer lines, which reaches 5700 km s^{-1}. Zheng & Keel (1991) reported an average Fe II $\lambda 4570/\mathrm{H}\beta$ ratio of 0.35 in their sample of 85 AGNs with FWHM between 2000 and 6000 km s^{-1}. They found an anticorrelation between the Fe II $\lambda 4570$ strength and the Hβ line width and no evidence of enhancement of optical Fe II with very broad lines. Also, none of the strong optical Fe II emitters listed in Table 4 of Lípari et al. (1993) shows line widths larger than 5300 km s^{-1}, confirming the particularity of the F10.01 galaxy in the sense of showing simultaneously strong optical Fe II and broad Balmer lines. This issue will be addressed in detail in § 4.1.

After subtraction of the Fe II template, there is still a continuum feature beginning to rise around 3900 Å and extending toward shorter wavelengths. This excess of emission is also present, with much greater intensity, in the A08.12 spectrum. The origin of this deviation will be discussed in the following section.

3.3. *The Balmer Continuum Emission*

The most important continuum feature present in the A08.12 spectrum is the remarkable near-UV excess extending from 4200 Å and blueward (see Fig. 3*a*). It is also present, with less intensity, in F10.01. We associated this continuum with both the Balmer continuum emission (Bac), originated by free-bound transitions to level 2 of the hydrogen atom, and to the merging of high-order Balmer lines. Observationally, the Bac is constrained to the interval between 3646 Å, where it reaches its maximum value, and 1400 Å, where it goes to zero intensity, but the inclusion of broad, blended, high-order Balmer emission lines broadens the sharp turn-on at $\lambda 3646$ and give the composite emission the shape of a bump with a peak near 3646 Å.

In order to isolate this feature, we followed the method and Bac templates (which includes the high-order Balmer lines) modeled by WNW. The best-matching model was scaled to and subtracted from the F10.01 and A08.12 spectra.

Our Balmer continuum flux measurements give a ratio $I(\mathrm{Bac})/I(\mathrm{H}\beta)$ of 1.6 and 9.2 for F10.01 and A08.12, respectively. I(Bac) corresponds to the flux measured in the range (3200–4000 Å). Since the Bac templates are calculated to cover the full wavelength interval of this continuum (1400–3646 Å), we can use the adjusted template to make some crude predictions about the total flux of this emission. We obtained $I(\mathrm{Bac\ total})/I(\mathrm{H}\beta)$ equal to 2.5 and 15 for F10.01 and A08.12, respectively. For A08.12, this ratio is almost twice the average found by WNW in their sample of nine AGNs, while for F10.01 it is about 3 times lower. The observed Bac flux in A08.12 is already too large when compared with optically thick models (Fig. 1 of WNW), suggesting $\tau_{(\mathrm{Bac})} \ll 1$, which in turn implies high effective Balmer continuum temperatures. If this is true, collisional ionization and related processes may be present, since they tend to enhance the Bac flux.

Figures 2 and 3 illustrate the final result of the continuum decomposition applied to F10.01 and A08.12. The observed spectra and the adopted power law are shown in the upper panel. Then, with this underlying continuum subtracted, the spectra and the model are superposed. Finally, the individual templates of the models are shown.

At this point, it is important to evaluate the sources of errors that may affect the measurements of the continuum decomposition carried out in both galaxies. We consider that the largest source of uncertainty lies in the definition of the power-law, since the underlying continuum may have a contribution from the stellar population. If we assume that the host galaxy of both Seyfert galaxies can be represented by an early-type spiral composed of a combination of blue and red stellar population and use the equivalent widths of an appropriate template (S6, from Bica 1988), we find that this contribution is not larger than 10% of the total continuum flux at 5870 Å in F10.01 and A08.12. With this in mind, the value of the spectral index α is not altered beyond the quoted errors of the PL fit by subtracting the above percentage of stellar population. Therefore, our results are not significantly affected by the contamination introduced by the host galaxy.

In order to determine how much the uncertainties in the power-law fit affect the Bac and Fe II fluxes, we subtracted power-law functions having the upper and lower values of α found for each galaxy and then estimated the integrated flux of each continuum feature. As Table 1 shows, an uncertainty of 5% in the spectral index of the PL (determined from the *nfit1d* task) in F10.01 leads to an uncertainty of 7% in the Fe II flux and up to 36% in the Bac measurement. In A08.12, the uncertainty in the Bac flux is lower, since no subtraction of Fe II was necessary.

It is also possible that some Fe II residual exists after subtraction of the Fe II template because we are assuming that the relative intensities of the Fe II lines are equal to those in the I Zw 1 template. This approximation, however, seems to be valid in most of the galaxies with Fe II emission, as discussed by Boroson & Green (1992) and corroborated not only with their sample but also in many other galaxies.

Table 1 lists (in ergs s^{-1} cm^{-2}) the integrated flux of each continuum component found in both galaxies.

4. THE EMISSION-LINE PROFILES

Prior to measuring the flux of the emission lines, we removed the underlying power law, the Balmer continuum, and the Fe II components. The integrated flux and FWHM of the emission lines were measured assuming that they were well represented by Gaussian profiles. The LINER routine, which fits as many as eight Gaussians to a line profile, was used for this purpose. For blended lines such as Hβ + [O III] $\lambda\lambda 4949$, 5007 and Hα + [N II] $\lambda\lambda 6548$, 6584, theoretical line ratios and known fixed wavelength separations between forbidden lines were used. In some cases it was necessary to adjust up to three Gaussians (identified as narrow, broad, and very broad components) to the permitted lines in order that the synthetically calculated blended

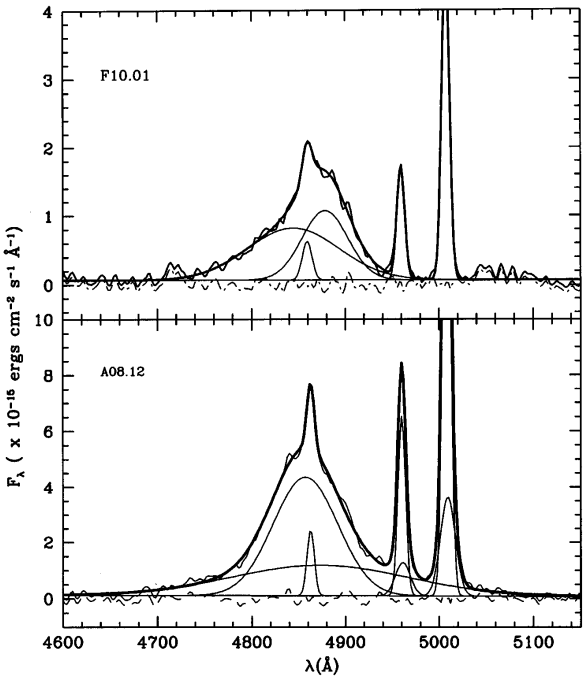

FIG. 4.—Example of the deblending procedure applied to the Hβ region in F10.01 (*upper panel*) and A08.12 (*lower panel*) after removing the continuum contribution. The dashed line corresponds to the residual of the fitting.

profile satisfactorily matched the observed profile. In A08.12, in addition to the narrow components, the [O III] lines were successfully reproduced by fitting an "intermediate" component to the base of the lines. Figure 4 shows an example of the Gaussian deblending procedure applied to the Hβ region in both spectra. The narrow, broad, very broad, and intermediate components of the lines can be easily identified. A strong blue wing in the Hβ profile of F10.01 is clearly visible in this figure. In order to check whether it was not a result of some Fe II residual, we compared the Hα to the Hβ profile normalized to unity, as shown in Figure 5. Note the great similarity between the two profiles, meaning that the Fe II subtraction did not modify the wing structure of the lines. It can also be seen that the blue wing extends at zero intensity up to −10,000 km s^{-1}, while the red one goes up to 5000 km s^{-1}, denoting a highly asymmetric profile. This asymmetry clearly indicates systematic motion of the broad-line emitting clouds combined with preferential viewing of different parts of the BLR. The blue wing could be caused by outflowing clouds in which the far side is partially shielded from sight, or infalling clouds in which the emission arises predominantly from the side of the clouds facing the central continuum source (Boroson & Green 1992).

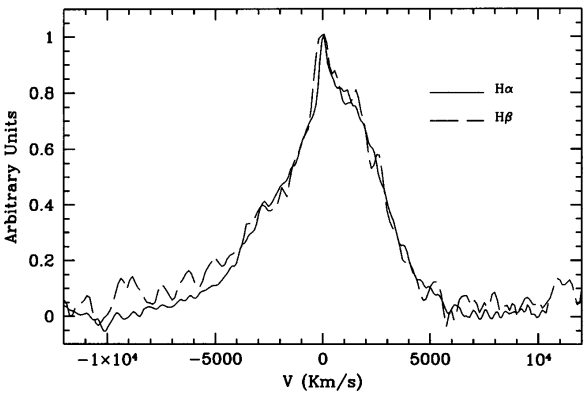

FIG. 5.—Comparison in space velocity between the Hα and Hβ line profiles, normalized to unity, for F10.01. The underlying Fe II emission has been subtracted. Note the strong blue asymmetry in the lines, denoting the presence of radial motion in the BLR of the galaxy (see text).

A08.12 is remarkable for the width of the lines He I λ5876 and He II λ4686, reaching a FWHM of order 10,000 km s^{-1}. Initially we were inclined to treat the strong bump blueward of Hβ as a mixture of Fe II and He II, but since no evidence of Fe II is observed on the red side of Hβ (i.e., emission from the Fe II multiplets 48 and 49, centered on 5250 Å), we discarded the presence of Fe II in the spectrum and regarded this emission as produced solely by He II.

Separating He II λ4686 from Hβ, however, is not simple. The red wing of the former is extremely blended with the blue side of the latter. The procedure adopted in this case consisted in isolating the velocity profile of He I λ5876 and using it as a template for He II λ4686. The height and width of the template were adjusted to produce the smoothest broad-line residual after subtraction. The fact that He I λ5875 and He II λ4686 are broader than Hβ is consistent with the work of Osterbrock & Shuder (1982) on low-luminosity AGNs. They found that the He I and He II lines were broader than the Balmer lines in most of the objects in which the He lines were visible.

The measured line fluxes and FWHMs of the lines for F10.01 and A08.12 are shown in Table 2. The statistical errors are derived from χ^2 fitting of the Gaussian models to the data, assuming that the pixel-to-pixel variation is due to random Gaussian noise. Measurement uncertainties for most of the emission lines are smaller than 10%. For fainter lines, such as Hδ (narrow), [Fe VII] λ6087, He I λ5876 (narrow), the uncertainties are about 10%–20%. In some cases, such as [O III] λ4363 and He II λ4686 (narrow), the uncertainties are greater than 20%.

In order to correct the observed narrow-line fluxes for internal extinction, we calculated the Balmer decrement Hα (n)/Hβ (n) assuming a theoretical ratio of 3.1. No evidence for reddening was found in either of the two galaxies.

4.1. *Broad-Line Region: Inferred Physical Conditions*

It is important to discuss the implications that our measurements of Fe II and Bac carried out in § 3, and the results of the emission-line profiles, have on the geometry and physical conditions of the BLR gas. We have seen that in F10.01 there is strong Fe II emission, up to the point of considering it as a strong Fe II emitter. In A08.12 instead, there is no evidence of Fe II, at least in the optical region. The opposite is true for the Balmer continuum, which is strong in A08.12 and weak in F10.01. Nonetheless, both galaxies have similar power-law spectral indices (see § 3.1) and FWHM of the Balmer lines (see Table 2).

Our observations largely favored the scenario proposed by Netzer (1987) in order to explain the BLR structure in F10.01 and A08.12. It consists of BLR clouds illuminated by a thin disk emitting anisotropic UV radiation combined with an isotropic X-ray source. Individual BLR clouds of number density N are situated at a distance R from the center of the disk at an angle θ as measured from the normal to the surface of the disk. Photoionization model calculations carried out by Netzer (1987) using this configuration to investigate the emergent emission-line spectrum reveal

TABLE 2

EMISSION-LINE FLUXES AND FWHMS OF THE LINES IN F10.01 AND A08.12

LINE	F10.01		A08.12	
	Flux[a]	FWHM[b]	Flux[a]	FWHM[b]
[Ne v] λ3425	14.5	1006	32.0	960
O III λ3443	...	...	0.7[c]	963
[O II] λ3727	5.9	616	25.0	680
[Ne III] λ3869	6.9	775	42.7	878
He II + He I + H8 λ3892	...	...	12.7	1159
[Ne III] λ3968	2.6	775	16.6	878
[S II] λ4070	...	...	13.0	543
Hδ (n)[d] λ4101	1.2[e]	500	9.7	913
Hδ (b)	29.5	5402	74.2	5883
Hγ (n) λ4341	7.5[e]	1055	20.2	905
Hγ (b)	45.9[e]	6457	145.9	5790
Hγ (vb)	...	...	90.3	12462
[O III] λ4363	2.2	950[e]	21.2[c]	1040
He II (n) λ4686	2.5[f]	699	4.6[e]	694
He II (b)	...	...	119.5	12722
Hβ (n) λ4861	6.1	740	22.7	562
Hβ (b)	61.4	3503	366.1	4993
Hβ (vb)	92.1	7117	253.5	13537
[O III] (n) λ5007	56.3	575	196.7	579
[O III] (i)	...	...	70.3	1128
He I (n) λ5876	1.1[c]	373	2.1[e]	300
He I (b)	21.0[e]	5837	51.5	5040
He I (vb)	...	...	101.6	12722
[Fe VII] λ6087	5.6[e]	1391	4.4[f]	412
[O I] λ6300	1.8[c]	350	16.6	713
[S III] λ6313	1.8[c]	350	4.9[g]	700
[Fe X] λ6374	0.5[g]	...	1.3[f]	300
[N II] λ6548	3.0	320	...	...
Hα (n) λ6563	17.4	461	70.5	456
Hα (b)	181.0	3366	1966.0	4389
Hα (vb)	539.0	6401	...	...
[N II] λ6584	9.0	320	...	...
[S II] λ6717	3.7[b]	305	8.5	401
[S II] λ6731	3.4[c]	305	9.1	401

[a] In units of 10^{-15} ergs s^{-1} cm^{-2}. Errors in fluxes are less than 10% unless otherwise indicated.

[b] In km s^{-1}. Errors are less than 10% unless otherwise indicated.

[d] (n), (i), (b), and (vb) indicate narrow, intermediate, broad, and very broad components, respectively.

[e] Error between 10% and 20%.

[c] Error between 20% and 30%.

[f] Error between 30% and 50%.

[g] Upper limit.

interesting trends. Small-θ clouds would produce strong Lyα, C IV λ1549, O VI λ1035, He I λ5876, and Balmer continuum emission, while large-θ clouds would emit strong low-excitation lines, such as C III] λ1909, Mg II λ 2798, and Fe II. Hα/Hβ would increase with increasing θ, from 2 (and even less for $N > 10^{10}$ cm^{-3}) to very large (> 10).

According to the above model, the BLR features observed in F10.01 can be understood in terms of emission coming predominantly from large-θ clouds while in A08.12 emission from small-θ clouds dominates. This by no means implies concentration of clouds at either large or small angles within the BLR, although this possibility is not discarded (Netzer 1987). The clouds may be arranged over a large distribution of angles, but only emission from clouds located in a particular angular interval is favored, owing to orientation effects of the disk relative to the observer.

Additional observational evidence supporting this picture are (1) the strong He I λ5876 and symmetric Balmer lines in A08.12, both compatible with small θ; (2) the pronounced asymmetry toward the red of the H I lines and the weak He I λ5876, facts predicted by the model for expanding systems viewed at large θ, as would be the case for F10.01; (3) the increase in Hα/Hβ from 3.1 in A08.12 to 4.7 in F10.01.

Also, some interesting predictions can be made for these two galaxies in accordance with the present model. It would be expected that F10.01 show strong C IV λ1909 and Mg II λ2798 lines as well as an asymmetric Lyα profile. In A08.12 the model predicts strong and symmetric Lyα, C IV λ1549, and O VI λ1035. We should be aware, however, of the very limited range in wavelength we are observing, which prevents us from drawing very accurate conclusions regarding the physical state of these two galaxies. It is clear that F10.01 and A08.12 are very valuable objects in relation to their continuum properties, and additional observations at other spectral regions are needed in order to confirm or discard our predictions.

4.2. *Physical Conditions and Abundances in the Narrow-Line Region*

The narrow-line spectrum of the observed galaxies shows a strong degree of ionization as deduced by the presence of numerous high-excitation lines such as [O III] λ5007, [Ne III] λ3869, [Ne V] λ3425, [Fe VII] λ6087, and [Fe X] λ6374. Of particular interest is the large value of the ratio $R_{[O\,III]}$ = [O III] λ4363/[O III] λ5007, which is equal to 0.04 and 0.09 in F10.01 and A08.12, respectively. The [O III] temperatures ($T_{[O\,III]}$) inferred from these ratios (22,000 ± 4000 and 40,000 ± 8000 K) far exceed the equilibrium temperature of photoionization models calculated with electron densities $n_e < 10^4$ cm^{-3} and solar abundance. It is worth mentioning that the "mean" observed Seyfert spectrum adopted for comparison by Ferland & Osterbrock (1985) has $R_{[O\,III]} = 0.019$ (i.e., $T_{[O\,III]} \sim 15{,}000$ K in the low-density regime). The density in the [S II] zone, derived by the [S II] λ6717/λ6731 ratio, is quite normal for the NLR of Seyferts, reaching 1300 ± 200 cm^{-3} in F10.01 and 800 ± 100 cm^{-3} in A08.12, assuming a temperature of 10^4 K.

Figure 6 illustrates the deblending procedure applied to the Hγ + [O III] λ4363 complex in A08.12. From this plot, it is clear that the observed high $R_{[O\,III]}$ ratio cannot be due to an inadequate deblending of these lines. Also, the effect of contamination by starlight on the strength of [O III] λ4363

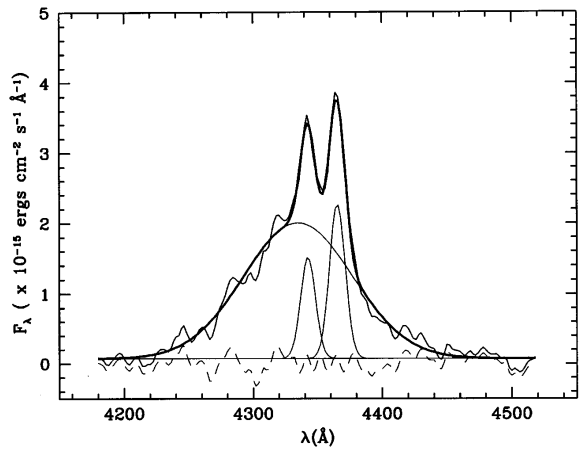

FIG. 6.—Deblending procedure applied to the Hγ + [O III] λ4363 complex in A08.12. Note the red side of the [O III] λ4363 profile, which has no observable changes in its structure from the base to the top of the line.

is considered negligible, since the stellar component is almost diluted by the strong nonstellar continuum emitted by the Seyfert nucleus, as explained in § 3. We therefore conclude that the abnormal high temperatures deduced for the NLR of F10.01 and A08.12 must have a physical origin rather than be caused by an error measurement.

The high values of $T_{[O\ III]}$ found above suggest the presence of gas in the NLR with densities around or greater than the critical density for the [O III] λ4959 and [O III] λ5007 lines, i.e., $n_e \gtrsim 10^6$ cm^{-3}. De Robertis & Osterbrock (1984, 1986) had already pointed out that the NLR presumably consists of clouds with a wide range in densities, possibly as high as 10^6 cm^{-3}. According to their hypothesis, the NLR would be composed of a region of low-density gas ($n_e \lesssim 10^4$ cm^{-3}), where most of the low- to intermediate-ionization lines are emitted, and a high-density region ($n_e \gtrsim 10^6$ cm^{-3}), responsible for the emission of high-ionization lines including the [O III] lines. The above picture is rejected by Moore & Cohen (1994) and Moore, Cohen, & Marcy (1996). They argue that emission-line profiles require significant emission in each line over most of the NLR, implying that line profiles of low and high critical density and/or low and high ionization potential might have similar width. It is not possible at this point to confirm or rule out this last hypothesis given the low resolution of our spectra and the low S/N of some of the high-ionization lines (e.g., [Fe VII] λ6087, [Fe X] λ6374), which prevent us from drawing reliable conclusions regarding correlations between critical density/ionization potential and line width. We may explore, however, possible scenarios for the NLR using the observed line ratios, as will be done in the following paragraphs.

In order to test the possibility of a stratified NLR, we have computed a grid of photoionization models using the code CLOUDY 84 (Ferland 1995). The adopted ionization continuum was "table AGN," similar to that deduced by Mathews & Ferland (1987) and consisting of a broken power law of the form $F_\nu = a\nu^{-\alpha}$ with α varying between 0.5 and 3 depending on the wavelength interval. Several sequences of models were computed by varying the ionization parameter U (defined as the quotient of the density of the impinging ionizing photons and the outer density of the gas cloud), the electron density n_e, and the metal abundance Z. We considered a range of densities ($n_H = 10^{2.5}$–$10^{6.2}$ cm^{-3}), ionization parameters ($U = 10^{-4}$ to 10^{-2}), and sulfur, nitrogen, and oxygen abundances (0.5–2) times the solar value. In Table 3 we have listed the observed line ratios along with the predicted line intensities relative to Hβ (narrow) from the best-matching model (high and low density) for each galaxy as well as the parameters characterizing the models.

It can be seen from Table 3 that only with the addition of a high-density NLR (i.e., $n_H \gtrsim 10^6$ cm^{-3}) is it possible to reproduce the observed $R_{[O\ III]}$ ratios, while the low- to intermediate-ionization lines are reasonably modeled assuming that they are produced in a region with n_H around 10^3 cm^{-3} and solar abundance. The above results are useful as a first approach, since they show us that the NLRs of both galaxies might indeed encompass a wide range in densities in order to reproduce successfully the observed line ratios. We then tried to calculate the output spectrum of a NLR cloud encompassing a wide range of densities, using CLOUDY 84, but we did not obtain much success in our modeling.

Binette, Wilson, & Storchi-Bergmann (1996, hereafter BWSB) considered an alternative picture in which there are two populations of photoionized clouds: a matter-bounded (MB) component responsible for most of the He II and high-excitation forbidden line emission, and an ionization-bounded (IB) component emitting low- to intermediate-excitation lines. The spectrum of the first population (MB) is determined from photoionization calculations truncated after a fraction F_{MB} of impinging ionizing photons has been absorbed. The excitation degree of this

TABLE 3

OBSERVED EMISSION-LINE SPECTRA OF F10.01 AND A08.12 COMPARED WITH PHOTOIONIZATION MODEL PREDICTIONS

	F10.01				A08.12			
LINE/PARAMETER (1)	Observed (2)	Low-Density Model (3)	High-Density Model (4)	MB-IB Model (5)	Observed (6)	Low-Density Model (7)	High-Density Model (8)	MB-IB Model (9)
[Ne V] λ3425.....	2.4	<0.1	<0.1	2.1	1.4	<0.1	<0.1	1.7
[O II] λ3737.....	1.0	5.4	0.1	3.3	1.1	3.3	<0.1	2.7
[Ne III] λ3868.....	1.1	1.2	2.5	0.8	1.9	1.1	2.8	1.4
[O III] λ4363.....	0.4	0.1	0.5	0.4	1.0	0.1	1.0	1.0
He II λ4686.....	0.4	0.2	0.1	0.3	0.2	0.2	0.1	0.3
Hβ.....	1.0	1.0	1.0	1.0	1.0	1.0	1.0	1.0
[O III] λ5007.....	9.2	9.0	9.0	9.2	11.8	12.6	11.8	11.7
He I λ5876.....	0.2	0.1	0.1	0.1	0.1	0.1	0.1	0.1
[Fe VII] λ6086.....	0.9	<0.1	<0.1	0.4	0.2	<0.1	<0.1	0.2
[O I] λ6300.....	0.3	0.3	0.4	1.0	0.7	0.3	0.2	0.8
Hα.....	2.9	2.7	2.8	2.8	3.1	2.7	2.8	2.8
[N II] λ6583.....	1.5	1.6	0.4	1.5	1.0[a]	0.3	0.1	1.3
[S II][b]	1.2	0.6	<0.1	1.3	0.7	0.4	<0.1	1.0
U	...	10^{-3}	10^{-3}	0.04[c]	...	$10^{-2.6}$	$10^{-2.6}$	0.04[c]
n_e (cm^{-3})	...	1200	10^6	3×10^5 [d]	...	1300	$10^{6.1}$	3×10^5 [d]
Z	...	Solar	Solar	Solar	...	Solar	Solar	Solar
$A_{M/I}$.....	...	...	...	1.5	...	...	...	2.5

[a] Upper limit.

[b] Sum of the fluxes of the doublet $\lambda\lambda$6717, 6731.

[c] U for the matter-bounded clouds.

[d] n_H for the matter-bounded clouds.

MB component is very high. The second population is much more opaque to the ionizing radiation and of much lower excitation. It is photoionized by the radiation that escapes the matter-bounded clouds. A sequence of line ratios is simply obtained by varying the relative proportion $A_{M/I}$ of the two distinct populations of photoionized clouds. In this approach, the high electron temperature $T_{[O\ III]}$ is properly accounted for, provided the thickness and ionization parameter of the MB component are appropriately selected. Also, much stronger high-excitation lines (e.g., [Ne V] λ3426 and C IV $\lambda\lambda$1549) are expected in this scheme, in accord with observations. This model was successfully applied by BWSB to the observed line ratios of the unresolved narrow-line region as well as to the extended emission-line region (EELR) (or the extended narrow-line region [ENLR]) of a sample of AGNs, which, otherwise, cannot be reproduced by conventional ionization-bounded photoionization calculations.

We have tested this approach using the photoionization code MAPPINGS IC (Binette et al. 1993b; Ferruit et al. 1997) to calculate the emergent NLR spectrum under a variety of conditions adopting the model of BWSB, i.e., a combination of high-excitation MB clouds and low-excitation IB clouds. The input spectrum of ionizing radiation consists of a canonical power law with index $\alpha = -1.3$. The ionization parameter U_{MB} of the MB component was chosen to be $U_{MB} = 0.04$ for F10.01 and A08.12, which allows us to obtain high electronic $T_{[O\ III]}$ temperatures (somewhat higher than in BWSB, because of our much higher density). A density $n_{MB} = 3 \times 10^5$ cm^{-3} was used for the MB region. This gives us a total gas pressure for the front layer equal to $P_{MB} = 1.95 \times 10^{10}$ K cm^{-3}, where K is the Boltzmann constant. The density behavior of the gas is isobaric, that is, constant pressure within both the MB component (of pressure P_{MB}) and the IB component (of pressure P_{IB}).

BWSB imposed a density increase of 20 for the pressure P_{IB} relative to P_{MB} on the grounds that the IB component corresponded to the dense core of photoionized clouds. This resulted in a low-excitation IB component, required in their line-fitting procedure of NLR and ENLR ratios. We here explore the alternative geometry of having the IB component situated at much larger radii from the source (cf. Fig. 4*a* in BWSB). The low excitation of the IB clouds in this case is the result of a larger geometrical dilution (higher radius from the nucleus) of the ionizing radiation that has filtered through the MB component. As for the pressure, the [S II] densities inferred from the λ6717/λ6731 ratio require that P_{IB} be much smaller than P_{MB} by a factor of $\sim 10^3$ cm^{-3}.

Since the excitation (U) of the gas depends on both the density and the dilution of the nuclear radiation, it is fairly straightforward to reproduce the same drop in U (i.e., excitation) as in BWSB, of a factor of 20 between the MB and IB components. This is done by simultaneously diluting (dividing) the radiation escaping the MB component by a factor $20^{1+\kappa}$ and dividing the pressure by a factor 20^{κ} (i.e., $P_{IB} = P_{MB}/20^{\kappa}$). We found that $\kappa = 2.3$ resulted in a reasonable fit of the [S II] densities. This implies that the IB component is at a radius $20^{(1+\kappa)/2} = 140$ times larger than the dense MB component, not unreasonable given that the slit widths had projected sizes of 1500 and 600 pc for F10.01 and A08.12, respectively. Solar abundance is assumed for the gas, and the calculations use a constant dust-to-gas ratio of $\mu = 0.015$ (in units relative to the solar neighborhood $\mu = 1$), which has a negligible effect on the line transfer. Depletion of the gas-phase metals is taken into account following the prescription given by Binette et al. (1993a).

Columns (5) and (9) of Table 3 present the predictions of line ratios calculated under the above set of conditions. It can be seen that they are in better agreement with the measured values of line ratios in F10.01 and A08.12 than those predicted by CLOUDY. According to our results, the observed NLR differences between the two galaxies can be interpreted as due to the variation of the relative proportion of MB and IB clouds inside the NLR. No gas having subsolar abundance is needed, as was recently suggested by Komossa & Schulz (1997), in order to reproduce the high $R_{[O\ III]}$ ratios observed. The ensemble of clouds cover a significant range in density, ranging from $n_H = 10^2$–10^6 cm^{-3} the MB component being dominated by the highest densities and the IB clouds by the lower ones. We may therefore conclude that the presence of MB and IB clouds in the NLR of F10.01 and A08.12 is another viable possibility to explain the high $T_{[O\ III]}$ temperatures and high-ionization lines observed in the narrow-line spectrum of these two galaxies. Of course, considering only two populations of clouds is certainly an oversimplification of the complex geometry characterizing the NLR, and such a simple scheme would not be applicable to AGNs with strong correlations between line widths and critical density.

5. SUMMARY AND CONCLUSIONS

We have analyzed optical data for the two newly detected Seyfert 1 galaxies F10.01 and A08.12. The data consist of long-slit spectra in the rest-wavelength region 3200–7000 Å at a resolution of 8 Å. Analysis of the observations led to the following conclusions:

1. The continuum energy distribution in F10.01 can be described as a combination of a steep nonstellar continuum of power-law form with spectral index $\alpha = -1.1$, Balmer continuum emission, and the pseudocontinuum formed by the merging of numerous Fe II emission multiplets. In A08.12, a power law with $\alpha = -1.2$ and strong Balmer continuum emission compose the observed continuum emission.

2. We found that F10.01 is a strong Fe II emitter (Fe II λ4570/H$\beta = 0.9 \pm 0.1$), has broad (FWHM $\sim$ 5700 km s^{-1}) and asymmetric emission Balmer lines and weak Bac [I(Bac)/I(Hβ)] = 1.6. A08.12 shows a strong Bac [I(Bac)/I(Hβ)] = 9.2, symmetrical H I profiles, and no Fe II. These spectroscopic properties can be explained in terms of BLR clouds illuminated by a thin disk, which emits anisotropic UV radiation, and an isotropic X-ray source. Such a scheme produces an angular dependence of the emission-line intensities. The BLR spectrum in F10.01 might be dominated by emission from large-θ clouds, while in A08.12 emission from small-θ clouds might be favored.

3. The NLRs of F10.01 and A08.12 are characterized by the presence of strong high-ionization forbidden lines and large $R_{[O\ III]}$ ratios. A NLR model composed of ionization-bounded clouds with densities in the interval $n_H = 10^4$–10^6 cm^{-3}, solar abundance, and a single ionization parameter for the entire cloud cannot fully reproduce the observations. A more detailed modeling of the NLR consisting of a combination of matter-bounded clouds of density in the range $n_H = 10^5$–10^6 cm^{-3} and ionization-bounded clouds having

a density interval $n_H = 10^2$–10^4 cm^{-3}, of much lower excitation, ionized by the radiation escaping the MB and 140 times more distant from the central source than the MB clouds, can better account for the observed line ratios and $T_{[O\ III]}$ temperatures.

We thank Beverly Wills for kindly providing the Fe II and Balmer continuum templates, and an anonymous referee for helpful suggestions to improve this paper. A. R. A. and M. G. P. gratefully acknowledge Luc Binette for fruitful discussions and invaluable assistance, and for making the code MAPPINGS IC available to us. This work has been partially supported by the Brazilian Research Council CNPq to A. R. A. and by the Chilean institution Fondo Nacional de Ciencias (FONDECYT) under grant 92-1083 to J. M.

REFERENCES

Bica, E. 1988, A&A, 195, 76
Binette, L., Wang, J. C. L., Villar-Marín, M., Martin, P. G., Magris, C. M. 1993a, ApJ, 414, 535
Binette, L., Wang, J. C. L., Zuo, L., & Magris, C. M. 1993b, AJ, 105, 797
Binette, L., Wilson, A. S., & Storchi-Bergmann, T. 1996, A&A, 312, 365 (BWSB)
Boroson, T. A., & Green, R. 1992, ApJS, 80, 109
Burstein, D., & Heiles, C. 1984, ApJS, 54, 33
Collin-Souffrin, S., Dumont, S., Joly, M., & Péquignot, D. 1986, A&A, 166, 27
DeRobertis, M. M., & Osterbrock, D. E. 1984, ApJ, 286, 171
———. 1986, ApJ, 301, 727
Ferland, G. J. 1995, HAZY: A Brief Introduction to CLOUDY (Univ. Kentucky Phys. Dep. Internal. Rep.)
Ferland, G. J., & Osterbrock, D. E. 1985, ApJ, 300, 658
Ferruit, P., Binette, L., Sutherland, R. S., & Pécontal, E. 1997, A&A, in press
Komossa, S., & Schulz, H. 1997, A&A, 323, 31
Kwan, J., Cheng, F.-Z., Fang, L.-Z., Zheng, W., & Ge, J. 1995, ApJ, 440, 628
Lípari, S., Terlevich, R., & Macchetto, F. 1993, ApJ, 406, 451
Marziani, P., Sulentic, J., Dultzin-Hacyan, D., Calvani, M., & Moles, M. 1996, ApJS, 104, 37
Mathews, W. G., & Ferland, G. J. 1987, ApJ, 323, 456
Maza, J., Ruiz, M. T., González, L. E., & Wischnjewsky, M. 1989, ApJS, 69, 349
———. 1992, Rev. Mexicana Astron. Astrofis., 24, 147
Maza, J., Ruiz, M. T., González, L. E., Wischnjewsky, M., & Antezana, R. 1994, Rev. Mexicana Astron. Astrofis., 28, 187
Moore, D., & Cohen, R. D. 1994, ApJ, 433, 602
Moore, D., Cohen, R. D., & Marcy, G. W. 1996, 470, 280
Netzer, H. 1987, MNRAS, 225, 55
Osterbrock, D. E., & Shuder, J. M. 1982, ApJS, 49, 149
Stone, R. P. S., & Baldwin, J. A. 1983, MNRAS, 204, 347
Wills, B., Netzer, H., & Wills, D. 1985, ApJ, 288, 94 (WNW)
Zheng, W., & Keel, W. 1991, ApJ, 382, 121